Controlling the quantum yield of a dipole emitter with coupled plasmonic modes

C. Vandenbem,[1] D. Brayer,[2] L. S. Froufe-Pérez,[3] and R. Carminati[2]
[1]*Research Center in Physics of Matter and Radiation (PMR), University of Namur (FUNDP), 61 rue de Bruxelles, 5000 Namur, Belgium*
[2]*Institut Langevin, ESPCI ParisTech, CNRS UMR 7587, 10 rue Vauquelin, 75231 Paris Cedex 05, France*
[3]*Instituto de Ciencia de Materiales de Madrid (CSIC) and Unidad Asociada CSIC-Universidad de Vigo, Calle Sor Juana Inés de la Cruz 3, 28049 Madrid, Spain*

(Received 29 November 2009; revised manuscript received 4 February 2010; published 26 February 2010)

We study theoretically the possibility of controlling the quantum yield of a single dipole emitter using coupled plasmonic modes. Plasmon hybridization offers spectral and spatial degrees of freedom that can be used to tune the spontaneous decay rate and the apparent quantum yield with high sensitivity. We demonstrate this concept on simple structures that could be implemented experimentally.

DOI: 10.1103/PhysRevB.81.085444 PACS number(s): 78.67.−n, 78.68.+m, 32.50.+d

I. INTRODUCTION

Advances in nano-optics have made possible the control of light-matter interaction processes on the nanometer scale. The control of spontaneous emission by single dipole emitters (e.g., molecules or quantum dots) is stimulated by applications such as the design of elementary sources for nanophotonics[1] or the use of spatially localized fluorescence signals for imaging.[2] The fluorescence features of a dipole emitter, such as the angular distribution of the emitted photons, the spectrum, and the fluorescence lifetime, can be strongly modified near plasmonic nanosystems. These systems are of interest in the context of single-molecule fluorescence since they produce intense and localized fields at the excitation frequency that are expected to increase the fluorescence signal. Nevertheless, the use of metallic structures induces the appearance of external nonradiative decay channels that can substantially reduce the apparent quantum yield. The interplay between local-field enhancement and radiative and nonradiative decay channels can lead to an enhancement of the fluorescence signal or to quenching.[3] Both situations are of interest regarding applications. Metallic nanoparticles of a few nanometers can be used as quenchers.[4,5] Such quenchers permit the design of activable fluorophores for *in vivo* molecular imaging, the activation being produced by a selective separation of quenchers and fluorescent centers.[6] On the other hand, enhancement of the fluorescence intensity can be obtained, for example, using nanoparticles with sizes on the order of 50–100 nm (Refs. 3 and 7) and has also been observed through continuous gold films supporting surface-plasmon polaritons.[8] An increase in the interaction distance up to 120 nm has also been demonstrated in fluorescence resonance energy transfer through similar films.[9] Initially driven by applications such as surface-enhanced Raman scattering,[10] local-field enhancement has been a subject of intensive research in plasmonics. For example, the local-field-enhancement factor has been evaluated close to nanoparticles and nanorods[11–15] or in tip-surface systems.[16] To the best of our knowledge, less attention has been dedicated to the study of the fluorescence quantum yield, although this quantity is at the center of both the fluorescence signal enhancement and the fluorescence quenching processes.

The possibility to tune the plasmon resonance in confined geometries offers new degrees of freedom for the control of the spontaneous emission features. This can be achieved using a resonant cavity, as a metallic disk on a substrate,[17] or an adjustable gap in a tip-sample geometry.[18] In this work, we discuss the following concept: The use of systems involving several coupled plasmon modes in order to act on the fluorescence quantum yield with high spatial sensitivity and spectral selectivity. The principle is as follows. The interaction between two (or more) metallic nanostructures gives rise to interesting hybridization of the plasmon modes,[14,19–24] in analogy to the chemistry of molecular orbitals. The spectrum of the coupled system exhibits eigenfrequencies corresponding to the eigenmodes, each eigenmode having its own spatial structure. As a result, the fluorescence quantum yield can be tailored using the spectral and spatial degrees of freedom.[22,25–27] Indeed, the coupling efficiency between the emitter and the plasmonic structure depends on the frequency matching between the emitted photons and the coupled modes spectrum, and on the spatial location of the emitter. When the coupled modes structure can be controlled by an internal parameter (e.g., distance between the nanoparticles in a dimer), we demonstrate theoretically the possibility of increasing or lowering the quantum yield by changing this internal parameter. It has been shown previously that the geometry of nanoparticles supporting plasmon resonances influence the quantum yield but modifying the shape of nanoparticles cannot be done in experiment with an external parameter.[26] Commonly, when a metallic structure is approached at nanometric distance to an emitter, its quantum yield is dramatically reduced. We show that this behavior can be overcome and that the quantum efficiency of an emitter can be increased when approaching a metallic object to the second object present in the geometry. This paves the way toward quantum efficiency manipulation at the nanoscale. We illustrate the general applicability of the concept on three different systems: a dimer of metallic nanoparticles, a thin metallic film, a hybrid system coupling a metallic film to a single metallic nanoparticle.

II. FLUORESCENCE QUANTUM YIELD

The apparent quantum yield η of an emitter (we use this denomination in opposition to intrinsic quantum yield) is an

important quantity that drives the fluorescence signal. It is defined by

$$\eta = \frac{\Gamma^R}{\Gamma^R + \Gamma^{NR}_{\text{int}} + \Gamma^{NR}}, \tag{1}$$

where Γ^R is the radiative decay rate that gives rise to the emission of a photon in the far field, Γ^{NR}_{int} is an intrinsic nonradiative decay rate that accounts for internal losses (e.g., vibrational relaxation in a molecule or nonradiative electron-hole recombination in a quantum dot), and Γ^{NR} is the external nonradiative decay rate induced by dissipation in an absorbing environment. The full decay rate Γ (inverse of the fluorescence lifetime) can be calculated from the electric-field susceptibility (the electric dyadic Green's function) of the system.[28] In order to compute the radiative and nonradiative decay rates Γ^R and Γ^{NR}, one can treat the transition dipole of the emitter as a classical harmonic damped electric dipole oscillating at the transition frequency. The radiative decay rate Γ^R is proportional to the power radiated in the far field, while the nonradiative decay rate Γ^{NR} is proportional to the power absorbed by the environment. The electric-field susceptibility as well as the radiated and absorbed powers can be computed by solving a classical radiation problem. The computation method that is used throughout this paper is summarized in the Appendix. The value of the intrinsic nonradiative decay rate Γ^{NR}_{int} depends on the type of emitter. In the present study, we have fixed arbitrarily $\Gamma^{NR}_{\text{int}} = \Gamma_0/2$, with Γ_0 the spontaneous decay rate in vacuum, which corresponds to an intrinsic quantum yield $\eta_{\text{int}} = 66\%$.

III. PLASMONIC DIMER SYSTEM

As a first example involving two coupled modes, we study a dimer made of two silver nanoparticles. The geometry is shown in the inset in Fig. 1(b). The dimer is composed of two identical spheres with radius r and an interparticle distance (measured from surface to surface) denoted by z_p. The emitter is placed along the dimer axis at a distance z_s from the surface of one nanoparticle. The transition dipole is assumed oriented along the dimer axis since this configuration offers the largest emitter-particle interaction.[29] In order to model the optical response of silver in the visible frequency range, we use a Drude model for the dielectric function $\epsilon(\omega) = \epsilon_\infty - \omega_p^2/(\omega^2 + i\omega\gamma)$ with parameters $\epsilon_\infty = 3.6$, $\omega_p = 1.42 \times 10^{16}$ Hz and $\gamma = 8.81 \times 10^{13}$ Hz.[30] This model is used for simplicity throughout this work to describe the dielectric function of silver. At very small emitter-surface distances z_s, microscopic corrections should be included through the use of a nonlocal dielectric function.[30,31] These corrections are not expected to change qualitatively the general trends when $z_s \geq 5$ nm.[32]

In a dimer, individual nanoparticle plasmons hybridize and give rise to bonding and antibonding combinations.[20–23] The eigenfrequencies corresponding to these two modes are shown in Fig. 1(a) versus the interparticle distance z_p for silver nanoparticles with radius $r = 5$ nm. At large separation z_p, and for a polarization of each particle along the dimer axis, the interaction is weak and one observes two degenerate

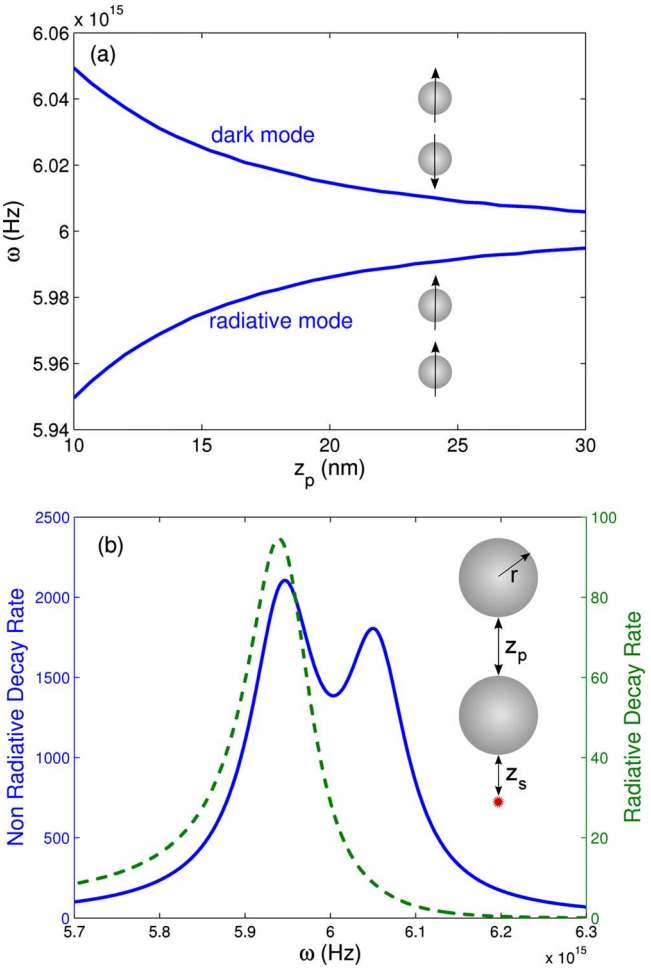

FIG. 1. (Color online) (a) Eigenfrequencies of the plasmonic dipole modes of a dimer of identical silver nanoparticles with radius $r = 5$ nm versus the distance z_p between the nanoparticles. The plasmon polarization is along the dimer axis. (b) Spectra of the normalized radiative decay rate Γ^R/Γ_0 (green dashed line) and nonradiative decay rate Γ^{NR}/Γ_0 (blue solid line) of a single dipole emitter located on the dimer axis at a distance $z_s = 5$ nm from the surface of one of the nanoparticles, with its transition dipole oriented along the dimer axis. The interparticle distance in the dimer is $z_p = 10$ nm. The geometry is shown in the inset.

modes at the plasmon frequency of an isolated particle. At small distance, a symmetric frequency splitting is observed, following a z_p^{-3} law typical of the dipole-dipole interaction that has been assumed in the calculation (for distances $z_p \geq r$, the electric dipole approximation is accurate enough to describe the lowest dimer plasmon mode[20]). The antibonding configuration [upper curve in Fig. 1(a)] corresponds to two dipole moments oscillating in-phase opposition so that the net dipole moment is zero for identical spheres. As a result, this mode is weakly coupled to radiation (dark mode). The frequency of this dark mode is above the plasmon frequency of an isolated nanoparticle. In contrast, the bonding configuration, with a frequency below the plasmon frequency of an isolated nanoparticle [lower curve in Fig. 1(a)], corresponds to two dipole moments oscillating in phase and is easily coupled to radiation (radiative mode).

The Green's function formalism allows us to derive analytical expressions of the radiative and nonradiative decay rates, as well as the apparent quantum yield η (see the Appendix for details on the method). In order to comply with the electric dipole approximation in the description of the dimer response, we keep $z_p \geq r$ and $z_s \geq r$ in all the calculations discussed in the following. The spectra of the normalized radiative (Γ^R/Γ_0) and nonradiative (Γ^{NR}/Γ_0) decay rates are shown in Fig. 1(b), for a distance $z_s=5$ nm between the emitter and the nanoparticle, and an interparticle distance $z_p=10$ nm in the dimer. The radiative decay rate (dashed green line) displays a resonance line shape centered at $\omega=5.95\times10^{15}$ Hz, corresponding to the coupling of the emitter with the radiative mode of the dimer. A peak value $\Gamma^R/\Gamma_0 \simeq 95$ is predicted at resonance. The nonradiative decay rate (solid blue line) shows a different line shape, with two peaks corresponding to a coupling to both the radiative and the dark mode of the dimer, the later leading to a resonance centered at $\omega=6.05\times10^{15}$ Hz. The enhancement of the nonradiative rate is much larger, with a peak value $\Gamma^{NR}/\Gamma_0 \simeq 2300$. These substantial differences between the behavior of both decay rates offer degrees of freedom for the control of spontaneous emission. This is a feature of the coupling to hybridize plasmonic modes.

The different behaviors of the radiative and nonradiative decay rates can be directly translated in terms of quantum yield. In particular, it is interesting to study the possibility of acting on the apparent quantum yield by changing an internal parameter of the dimer system, such as the interparticle distance z_p. This distance is a key control parameter since it drives the coupling strength between the plasmonic modes of the particles. Moreover, controlling this parameter is achievable experimentally, using dimers linked with chains of macromolecules such as peptides[4] or DNA,[33] or using near-field optical scanning microscopy (SNOM) techniques with, e.g., one particle attached at the apex of a near-field probe and the other particle deposited on a substrate (in this case the influence of the substrate might be non-negligible). The behavior of the apparent quantum yield η of a single emitter coupled to a dimer when the interparticle distance z_p is changed is shown in Fig. 2. More precisely, the maps show the value of η versus the position of the upper particle that scans a square region while the lower particle is fixed (see the geometry in the inset). The emitter is also fixed at a distance $z_s=5$ nm below the surface of the lower particle. In Fig. 2(a), the emission frequency is $\omega=6.05\times10^{15}$ Hz, corresponding to the right-hand side resonance peak in Fig. 1(b) (resonance involving the dark mode of the dimer). In Fig. 2(b), the emission frequency is $\omega=5.95\times10^{15}$ Hz corresponding to the left-hand side resonance peak in Fig. 1(b) (resonance involving the radiative mode of the dimer). We see that the behavior is substantially dependent on the emission frequency. In the case of Fig. 2(a), the emitter couples to the dark mode of the dimer so that the apparent quantum yield is strongly decreased with respect to its free-space value, due to nonradiative energy transfer to the metal mediated by the dark mode. When z_p decreases, mode splitting becomes more effective, thus reducing the (weak) coupling of the dark mode to the radiative mode. The radiative decay rate Γ^R is reduced while the nonradiative rate Γ^{NR} increases so that the apparent quantum yield is dramatically reduced. This leads to an efficient quenching of the fluorescence, with a quenching efficiency that depends on the control parameter z_p. The situation in Fig. 2(b) is more surprising. In this case, the emitter couples to the radiative mode of the dimer. We observe that a reduction in z_p induces a local increase in the apparent quantum yield, thus leading to a map exhibiting a contrast inversion with respect to that in Fig. 2(a). This is an unexpected behavior since with simpler system, as a flat surface or a single particle, one usually observes a monotonic decrease in the quantum yield as the emitter-system distance decreases.[3,34,35] Let us stress that even in the situation of contrast reversal, the absolute value of η remains much lower than the free-

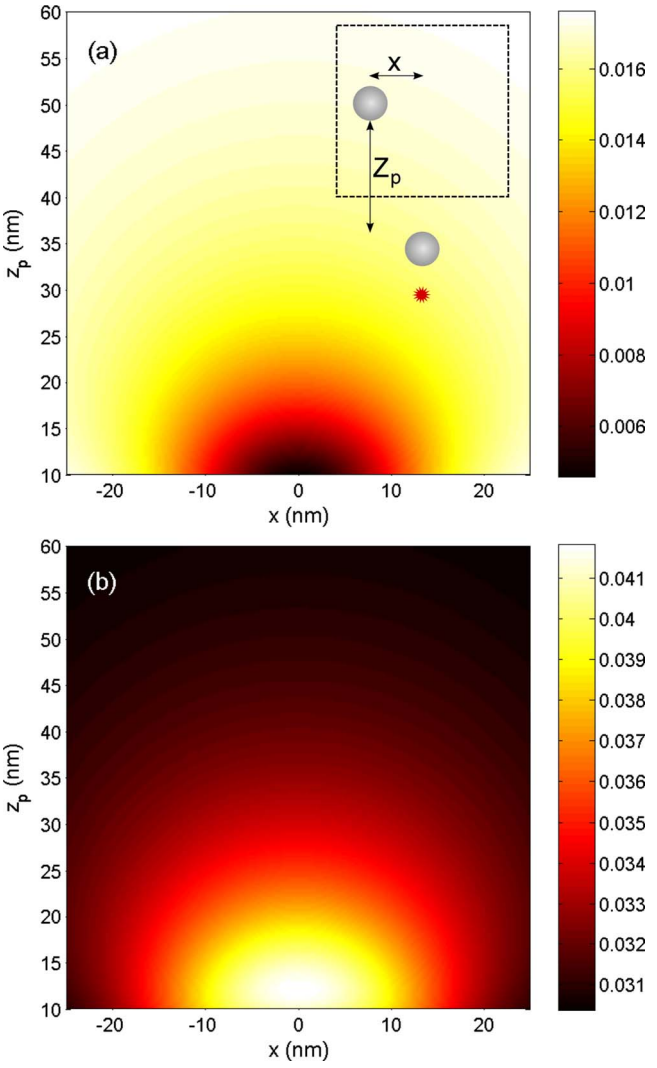

FIG. 2. (Color online) Maps of the apparent quantum yield of a single emitter located at a distance $z_s=5$ nm from the surface of one particle in a plasmonic dimer while the other particle scans a rectangular region (see the inset for the geometry). The emitter is located along the z axis, with its transition dipole oriented along the same axis. (a) Emission frequency $\omega=6.05\times10^{15}$ Hz corresponding to the right-hand side resonance peak in Fig. 1(b) (resonance associated to the dimer dark mode). (b) Emission frequency $\omega=5.95\times10^{15}$ Hz corresponding to the left-hand side resonance peak in Fig. 1(b) (resonance associated to the dimer radiative mode).

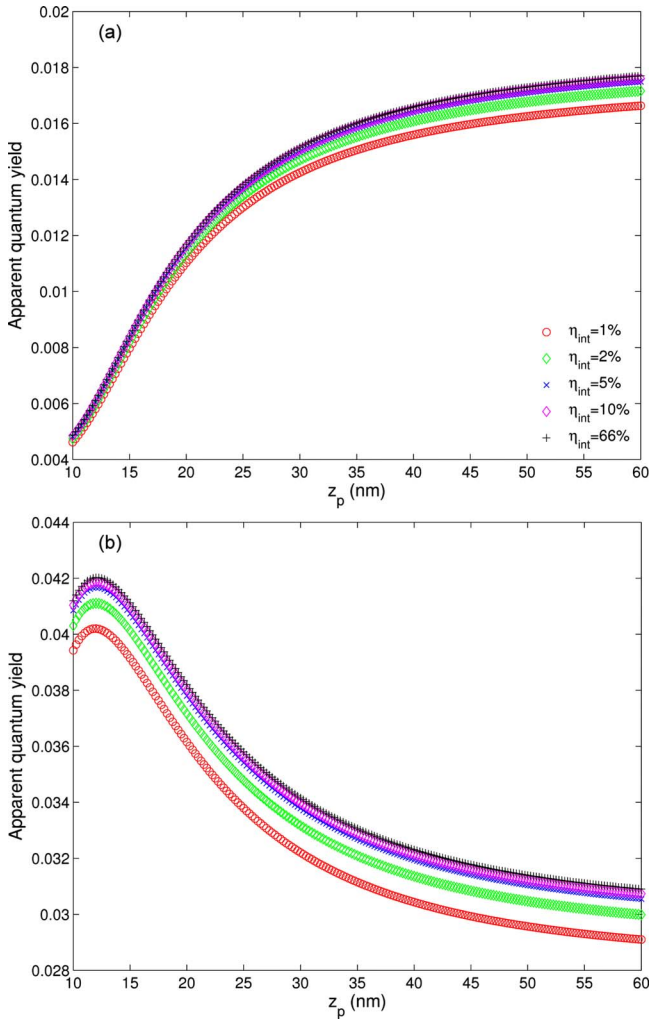

FIG. 3. (Color online) Apparent quantum yield of a single emitter with varying intrinsic quantum yield η_{int}, located at a distance $z_s=5$ nm from the surface of one particle in a plasmonic dimer versus the distance z_p between the nanoparticles. The legend gives the values of η_{int}. The emitter is located on the dimer axis, with its transition dipole oriented along the same axis. (a) Emission frequency $\omega=6.05\times10^{15}$ Hz corresponding to the right-hand side resonance peak in Fig. 1(b) (resonance associated to the dimer dark mode). (b) Emission frequency $\omega=5.95\times10^{15}$ Hz corresponding to the right-hand side resonance peak in Fig. 1(b) (resonance associated to the dimer radiative mode).

space value so that the overall situation remains that of a strong quenching. Our calculations demonstrate that the quenching efficiency can be modified by changing the geometrical parameters of the system.

It has been recently shown that resonant coupling to the plasmon modes of a metal sphere leads to an enhancement of the quantum yield of low-quantum-yield emitter (namely, that the apparent quantum yield η becomes larger than the intrinsic quantum yield η_{int}).[36] We have thus examined whether the intrinsic losses of the emitter (described by Γ_{int}^{NR}) influence the previous results. In the case of the dark mode [Fig. 3(a)], for strong internal losses ($\eta_{\text{int}}=1\%$) and for $z_p>20$ nm, we observe a weak enhancement. Nevertheless, coupling to the radiative mode is more advantageous for the enhancement of the quantum yield of emitter with strong intrinsic losses [Fig. 3(b)]. For $\eta_{\text{int}}=1\%$, the apparent quantum yield can reach 4%. The result is even more striking when we double the diameter (20 nm) of the spheres and the separation distances (20 nm). In this case, the apparent quantum yield tends to 25% (not shown for brevity). Such enhancement factors are identical to those obtained with a single sphere with a diameter of 60 nm.[36] We also observe in Fig. 3(b) that the maximum value of the apparent quantum yield saturates rapidly as the intrinsic quantum yield increases (saturation is observed as soon as $\eta_{\text{int}}\simeq10\%$).

Although not shown for the sake of brevity, we have also studied the angular radiation pattern of the dipole emitter coupled to the dimer system. This is done by computing the far-field radiation of a classical electric dipole located at the position of the emitter. The radiation pattern is also strongly dependent on the emission frequency. When the emitter couples to the radiative mode, the emission pattern is dipole-like, with a dipole orientation along the dimer axis. Conversely, we observe a more isotropic emission pattern for the emission wavelength corresponding to the dark mode. As expected, the radiated intensity in the far field is much larger with the radiative mode than with the dark mode (about 40 times larger for an emitter-particle distance $z_s=5$ nm and an interparticle distance $z_p=10$ nm in the case of the silver dimer).

IV. THIN METALLIC FILM

In the following, we shall demonstrate with other systems that the radiative and nonradiative decay rates can be triggered by an internal parameter determining the system geometry, thus illustrating the generality of the principle described previously in the case of the dimer. In the remainder of the paper, we consider emitters with an intrinsic quantum efficiency $\eta_{\text{int}}=66\%$. To proceed, we study the fluorescence characteristics of a single emitter close to a thin metallic film, which is a different system involving coupled plasmonic modes. We consider a thin silver film with thickness L, surrounded by air or vacuum, as shown in the inset in Fig. 4(a). Each metal-air interface supports resonant electromagnetic modes known as surface-plasmon polaritons. For a thick metal film (e.g., $L\geq100$ nm for silver), each interface supports the same surface-plasmon mode (twofold degeneracy). When L decreases, the modes start to interact due to the overlapping of their evanescent contributions inside the metal and a mode splitting is observed. The degenerate surface-plasmon mode splits into symmetric and antisymmetric modes (the nomenclature is defined with respect to the transverse electric-field distribution).[37] The eigenfrequency of each mode are plotted in Fig. 4(a) versus the film thickness L. The eigenfrequency of the symmetric (antisymmetric) mode increases (decreases) as the film is made thinner. Each mode is characterized by its own dispersion relation given by the following expression:[38]

$$\text{Symmetric:}\ \epsilon_m k_s + \epsilon_s k_m \tanh\left(\frac{k_m L}{2i}\right) = 0, \qquad (2)$$

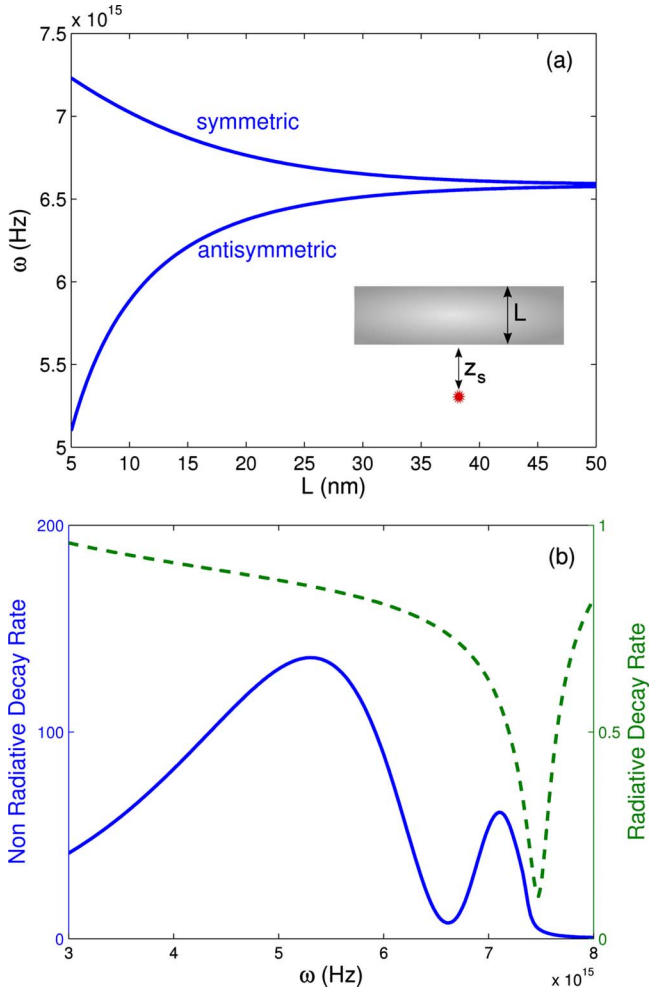

FIG. 4. (Color online) (a) Eigenfrequencies of the plasmonic modes of a thin silver film versus the film thickness L. The dielectric function $\epsilon_m(\omega)$ of the metal (silver) is described by a Drude model (Ref. 30) and the surrounding medium is vacuum or air with $\epsilon_s=1$. The mode splitting is visible when L decreases, leading to symmetric (upper branch) and antisymmetric (lower branch) modes. (b) Spectra of the normalized decay rates Γ^R/Γ_0 (green dashed line) and Γ^{NR}/Γ_0 (blue solid line) for a dipole emitter located at a distance $z_s=10$ nm from the film surface, with its transition dipole perpendicular to the interface. The thickness of the film is $L=5$ nm.

$$\text{Antisymmetric:}\epsilon_m k_s + \epsilon_s k_m \coth\left(\frac{k_m L}{2i}\right) = 0. \qquad (3)$$

The dielectric functions ϵ_m and ϵ_s correspond to the metal and the surrounding medium, and k_m and k_s are the normal components of the wave vector in the metal and in the surrounding medium, respectively. For a given value $k_\parallel$ of the wave vector parallel to the interfaces, one has $k_m=[(\omega/c)^2\epsilon_m-k_\parallel^2]^{1/2}$ and $k_s=[(\omega/c)^2\epsilon_s-k_\parallel^2]^{1/2}$, with the determination $\mathrm{Re}(k_m)>0$, $\mathrm{Im}(k_m)>0$ and $\mathrm{Re}(k_s)>0$, $\mathrm{Im}(k_s)>0$. Modes are spatially localized if k_s is purely imaginary, which corresponds to evanescent modes in the direction perpendicular to the interfaces. For the dispersion relation plotted in Fig. 4(a), we fixed $k_\parallel=6\times10^8$ m^{-1}. Note that both modes are dark modes since they do not radiate in the far field. But as we shall see, it is possible to take advantage of their different spatial structures to induce selective changes on the fluorescence decay rates of a dipole emitter coupled to the thin film.

We now study the spontaneous emission dynamics of an emitter located at a distance $z_s=10$ nm from a silver film with thickness $L=5$ nm [see the geometry in the inset in Fig. 4(a)], with its transition dipole oriented perpendicularly to the interface. The spontaneous decay rates can be computed from the dyadic Green's function of the film.[39] For such a slab structure, the Green's function is known analytically in Fourier space (angular spectrum decomposition).[40] In this formalism, surface-plasmon modes are accounted for without any approximation. The normalized radiative and nonradiative decay rates are plotted in Fig. 4(b) versus the emission frequency ω. In the spectrum of Γ^{NR} (blue solid line), one can identify two resonances corresponding to the coupling to the antisymmetric mode for $\omega\simeq5.5\times10^{15}$ Hz and to the symmetric mode for $\omega\simeq7.2\times10^{15}$ Hz. The coupling of the emitter to these dark modes leads to an enhanced nonradiative energy transfer to the metal film, with a stronger and broader resonance in the case of the antisymmetric mode. The behavior of the radiative rate Γ^R (green dashed line) is completely different. It is almost not affected by the antisymmetric mode while a sharp decrease in Γ^R is observed by coupling to the symmetric mode. As in the case of the dimer structure discussed previously, these different behaviors have strong implications regarding the apparent quantum yield since the tradeoff between radiative and nonradiative couplings is strongly dependent on the selected mode. When the thin film is excited by a dipole emitter placed in its near field, mode selectivity can be achieved using two parameters: the emission frequency ω and the distance z_s between the film and the emitter (we assume that the source polarization is fixed, with a transition dipole oriented perpendicularly to the film surface). When $z_s\ll\lambda$, a dipole emitter at a distance z_s illuminates the film surface with a quasistatic field with a lateral extension on the order of z_s (Ref. 41) and therefore selects a parallel wave vector $k_\parallel\sim2\pi/z_s$. Through the dispersion relation [Eqs (2) and (3)], one can deduce the associated eigenfrequencies of the modes that will be preferentially excited. In other words, the distance z_s selects the spectral position of the two resonance peaks of the nonradiative decay rate in Fig. 4(b).

Following the same line as in the dimer case, one could investigate the influence of an internal parameter (the film thickness L) on the decay rates and the quantum yield. Nevertheless, it seems that the thin-film geometry is not appropriate for at least two reasons. First, modifying the film thickness on the nanometer scale is not achievable experimentally in practical conditions. Second, we have observed in the calculations (not shown) that the effects are weak in terms of the control of the quantum yield and, in our opinion, without real interest in terms of experimental implementations. Nevertheless, it is possible to take advantage of the plasmonic modes of the thin film by adding another control parameter, namely, by coupling the film to a single nanoparticle, as we shall see in the next section.

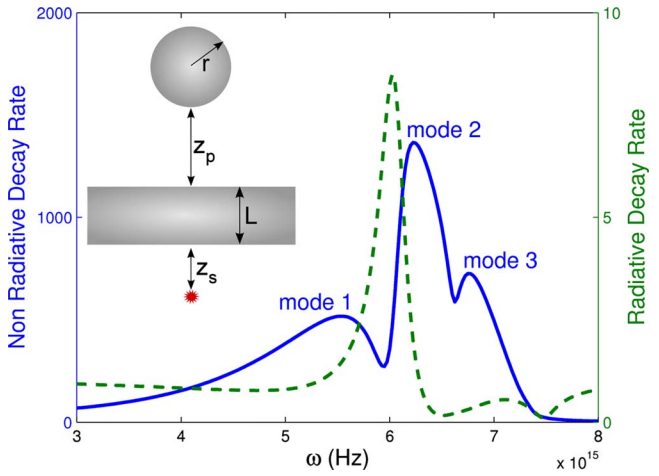

FIG. 5. (Color online) Spectra of the normalized decay rates Γ^R/Γ_0 (green dashed line) and Γ^{NR}/Γ_0 (blue solid line) for a dipole emitter located at a distance $z_s=10$ nm from the film surface, with its transition dipole perpendicular to the interface. The thickness of the film is $L=5$ nm. The radius of the nanoparticle is $r=5$ nm and the distance between the nanoparticle and the film surface is $z_p=5$ nm. The geometry is depicted in the inset.

V. MIXING PLASMONIC MODES: THE NANOSPHERE-FILM SYSTEM

The nanoparticle-film system that we consider is represented in the inset in Fig. 5. The silver film has a thickness L and the silver nanosphere has a radius r. The emitter and the nanosphere are placed on opposite sides of the film, the distance from the emitter to the slab surface being denoted by z_s and the distance from the nanoparticle surface to the slab surface being denoted by z_p. This scheme could be implemented experimentally, e.g., by fixing a single nanoparticle at the apex of a tip and controlling the tip-surface distance with standard SNOM techniques.

As in the previous cases, the spontaneous decay rates are obtained from the dyadic Green's function of the nanoparticle-film system, that is, computed self-consistently using the approach described in the Appendix. For simplicity in the present work, we have reduced the nanoparticle to a single electric dipole under the conditions $r \ll \lambda$ and $z_p \geq r$, λ being the emission wavelength. We show in Fig. 5 the normalized radiative and nonradiative decay rates Γ^R/Γ_0 (green dashed line) and Γ^{NR}/Γ_0 (blue solid line) for a dipole emitter located at a distance $z_s=10$ nm from the film surface, with its transition dipole perpendicular to the interface and a spherical nanoparticle with radius $r=5$ nm placed at a distance $z_p=5$ nm on the other side (see the geometry in the inset). The thickness of the film is $L=5$ nm as in Fig. 4(b). The spectrum of the nonradiative decay rate Γ^{NR} exhibits three resonances, each corresponding to a specific plasmonic mode of the coupled nanoparticle-film system.[24]

The origin of each mode can be deduced from the eigenfrequencies of the splitted (symmetric and antisymmetric) modes of the thin film and the resonance frequency ω_{sp} of the localized plasmon of the nanoparticle, defined by $\mathrm{Re}[\epsilon(\omega_{sp})]=-2$, with $\epsilon(\omega)$ the dielectric function of silver. Indeed, the low-frequency mode (mode 1) originates from the antisymmetric mode of the isolated film while the high-frequency mode (mode 3) originates from the symmetric mode. The resonance frequency of these modes is slightly shifted due to the interaction with the nanoparticle. The middle-frequency mode (mode 2) originates chiefly from the plasmon resonance of the isolated sphere that couples to the film interfaces. These interpretations are supported by the maps of the electric-field intensity inside the structure, presented on the left column in Fig. 6, when the system is illuminated by a classical electric dipole placed at the location of the emitter. In the case of mode 1 (top panel) and mode 3 (bottom panel), the intensity in the sphere is weaker than in

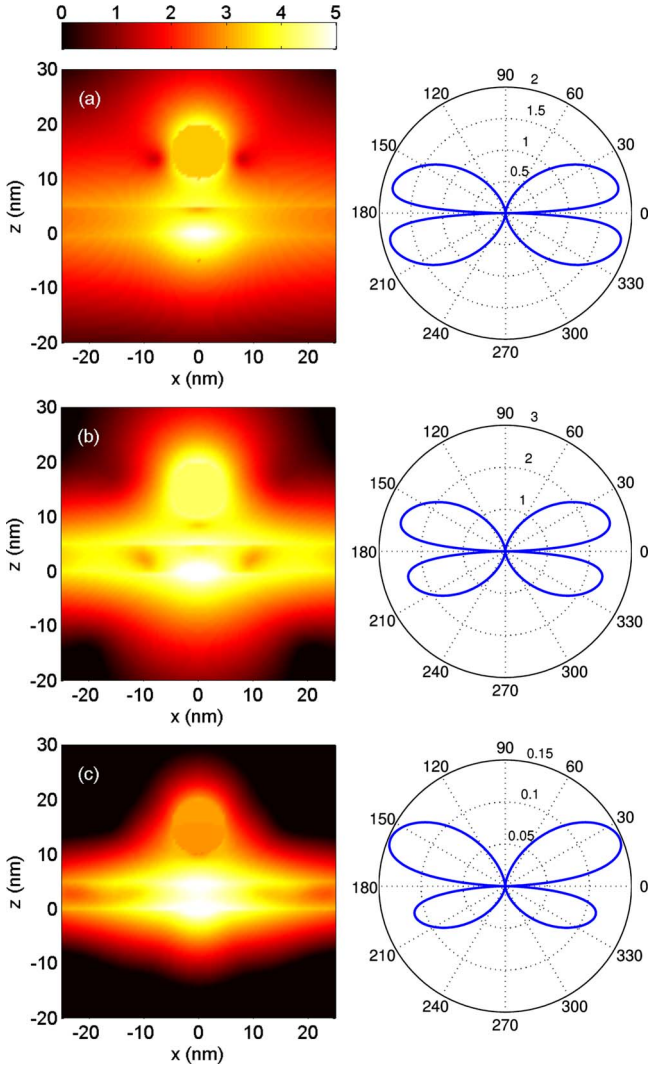

FIG. 6. (Color online) Maps of the electric-field intensity in arbitrary unit (color bar is of $\log|\mathbf{E}|^2$) in the emitter-film-nanosphere system at three emission frequencies corresponding to the three resonances identified in Fig. 5. (a) Mode 1 (generated by the antisymmetric mode of the thin film). (b) Mode 2 (generated by the localized plasmon resonance of the nanoparticle). (c) Mode 3 (generated by the symmetric mode of the thin film). The right column shows the far-field radiation patterns in each situation versus the observation angle in a vertical plane containing the emitter and the center of the nanoparticle (polar plot). 90° corresponds to the vertical emission.

the film (the sphere is off resonance) and the underlying antisymmetric (mode 1) and symmetric (mode 3) structures of the field in the film are still visible (although they are affected by the interaction with the nanoparticle). We recall here that the nomenclature of the mode of the thin film is given in accordance to the distribution of the transverse component of the electric field.[37] In Fig. 6, we plot the intensity of the total field and such representation explains the difference between the mode distribution and the nomenclature. In the case of mode 2 (middle panel), the high intensity inside the sphere is the signature of the excitation of its plasmon resonance. This plasmon resonance couples to the metallic film, creating a substantial field enhancement in the film. The field intensity inside the metals is responsible for the dissipation by Joule effect. In the case of mode 2 (middle panel), the field enhancement explains the high value of Γ^{NR} in the spectrum in Fig. 5. One also observes a weaker intensity inside the metallic film for mode 1 (top) than for mode 3 (bottom), which is in agreement with the relative heights of the other resonance peaks of Γ^{NR} in Fig. 5.

As far as the radiative decay rate Γ^R is concerned, the spectrum in Fig. 5 shows that its behavior is very different from that of Γ^{NR}. In particular, Γ^R exhibits only one resonance peak, slightly redshifted from the resonance of Γ^{NR} induced by mode 2 [mode associated to the localized plasmon of the sphere see Fig. 6(b)]. Such a redshift of Γ^R compare to Γ^{NR} has been already pointed out in a different configuration, involving an isolated metallic nano-object and a single molecule.[35] At the resonance frequencies of mode 1 and mode 2, Γ^R takes on similar values while it is much smaller at the resonance frequency of mode 3. This behavior is also seen on the radiation patterns (polar plots of the far-field radiated intensity) presented on the right column in Fig. 6. Although the patterns are very similar in the three cases, the level of radiated intensity is much weaker (about 15 times) in the case of mode 3 (bottom panel). Another feature of these radiation patterns is their relative symmetry with respect to the film plane. This means that half of the emitted photons could be collected on each side, which might represent an advantage from a practical point of view since various configurations could be implemented with similar collection efficiencies, e.g., with excitation detection on the same side or on opposite sides.

The relative behaviors of Γ^{NR} and Γ^R are very different from one mode to another. As in the case of the dimer structure discussed previously, one can expect the apparent quantum yield η to react in a specific manner to the modification of an internal parameter, when the emitter is coupled to a given mode. A natural internal parameter is the nanoparticle-film distance z_p that could be modified experimentally with nanometer-scale precision using SNOM techniques. The behavior of the apparent quantum yield η of a single emitter coupled to the nanoparticle-film system is shown in Fig. 7. The maps correspond to the value of η for each position of the nanoparticle that scans a rectangular region (see the geometry in the inset in the bottom panel). One sees that the quantum yield maps are very different for each emission frequency, i.e., the behavior of η is strongly dependent on the excited mode. In each case, the value of η is much smaller than that in free space (quenching regime) but the spatial

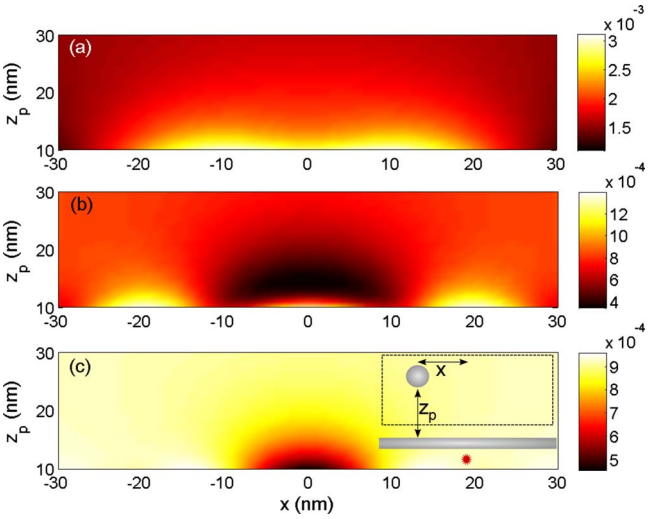

FIG. 7. (Color online) Maps of the apparent quantum yield η of a single emitter located at a distance $z_s=5$ nm from the lower surface of a silver thin film with thickness $L=5$ nm while a silver nanoparticle with radius $r=5$ nm scans a rectangular region on the other side (see the inset in the bottom panel for the geometry). The emitter transition dipole is perpendicular to the film surface. (a) Emission frequency corresponding to mode 1 in Fig. 5. (b) Emission frequency corresponding to mode 2. (c) Emission frequency corresponding to mode 3.

variation in η is the point of interest. For mode 3 (bottom panel), the apparent quantum yield decreases when the nanoparticle approaches the surface of the film above the emitter location. This is not surprising since, as we have seen, mode 3 is essentially nonradiative so that it mainly enhances the nonradiative energy transfer between the emitter and the metallic film. The case of mode 2 is on the overall similar, with a decrease in the quantum yield when the nanoparticle approaches the surface above the emitter. Note that the lateral extension of this mode, seen in Fig. 6 (left column, middle panel), generates a peculiar lateral structure. Indeed, the apparent quantum yield increases at small distances z_p when the nanoparticle is laterally shifted from the location of the emitter. The coupling to the low-frequency mode (mode 1, top panel) generates an unexpected behavior. The apparent quantum yield η increases when z_p decreases, this behavior being observed on a wide lateral scale. This contrast reversal in the quantum yield map is of the same nature as that discussed previously in the case of the dimer structure. In simple terms, our calculation demonstrate that for an emitter coupled to this mode and for a given exciting intensity, approaching the metallic nanoparticle to the film surface induces the emission of more photons. The photon emission can be triggered with a high sensitivity by changing an internal parameter on the nanoscale and with a lateral resolution that is driven by the lateral extension of the plasmonic mode (a few tens of nanometers in this example).

VI. CONCLUSION

In conclusion, we have introduced a concept that permits a control of the fluorescence quantum yield of a single dipole

emitter with high spectral selectivity and spatial sensitivity. The approach is based on the use of coupled plasmonic modes obtained by plasmon hybridization. Each mode having its specific frequency and spatial structure, the coupling efficiency between the emitter and the plasmonic structure can be tuned using the emission frequency and the emitter location as degrees of freedom. The interplay between radiative modes and dark modes offers the possibility of either lowering or increasing the quantum yield by changing an internal parameter of the system. We have illustrated the generality of the concept on three different examples: a dimer of metallic nanoparticles, a thin metallic film, and a hybrid system coupling a metallic film and a single metallic nanoparticle. The proposed schemes could be implemented experimentally using near-field optics or chemical self-assembly techniques.

ACKNOWLEDGMENTS

This work was supported by the EU Project *Nanomagma* under Contract No. NMP3-SL-2008-214107. C. Vandenbem acknowledges the Belgian National Fund for Scientific Research (FRS-FNRS) and a grant from the City of Paris that made possible a stay at ESPCI where part of this work was done. L.S. Froufe-Pérez acknowledges support from the Spanish Ministry of Science and Innovation through its Juan de la Cierva program.

APPENDIX: COMPUTATION METHOD

In the weak-coupling regime, the spontaneous decay rate Γ of a quantum emitter can be written as[28]

$$\Gamma = \frac{2}{\hbar}|\mathbf{p}|^2 \mathrm{Im}[\mathbf{u}\cdot\mathbf{G}(\mathbf{r},\mathbf{r},\omega)\cdot\mathbf{u}], \tag{A1}$$

where $\mathbf{r}$ is the emitter position, $\mathbf{p}$ its transition dipole, and $\mathbf{u}$ a unit vector in the direction of $\mathbf{p}$. The Green tensor $\mathbf{G}$ (or electric-field susceptibility) of the system connects the radiated electric field at position $\mathbf{r}'$ to a point source (electric dipole) $\mathbf{p}$ at position $\mathbf{r}$ through the relation $\mathbf{E}(\mathbf{r}',\omega) = \mathbf{G}(\mathbf{r}',\mathbf{r},\omega)\cdot\mathbf{p}$.

In free space, the vacuum Green tensor $\mathbf{G}_0$ is known analytically and one obtains $\Gamma_0 = \omega^3|\mathbf{p}|^2/(3\pi\epsilon_0\hbar c^3)$. In an arbitrary geometry, we write the full Green tensor as $\mathbf{G}(\mathbf{r}',\mathbf{r},\omega) = \mathbf{G}_0(\mathbf{r}',\mathbf{r},\omega) + \mathbf{S}(\mathbf{r}',\mathbf{r},\omega)$, where $\mathbf{S}(\mathbf{r}',\mathbf{r},\omega)$ is the modification of the vacuum Green tensor induced by scattering and absorption in the environment. In order to compute the decay rate, one has to compute $\mathbf{S}(\mathbf{r}',\mathbf{r},\omega)$, which is the solution of a classical radiation problem.

The systems considered in the present work involve spherical particles and slabs. In order to calculate numerically the scattering Green tensor $\mathbf{S}(\mathbf{r}',\mathbf{r},\omega)$, we first deal with the slab contribution. It can be obtained analytically by expanding the Green tensor into plane waves (angular spectrum representation).[40] This representation allows to describe both propagating and evanescent modes, and their interaction with the slab surfaces through Fresnel reflection and transmission factors. With this approach, the slab contribution $\mathbf{S}_{\mathrm{slab}}(\mathbf{r}',\mathbf{r},\omega)$ is obtained without any approximation. In particular, this part of the Green tensor includes the electromagnetic surfaces modes of the (laterally infinite) slab.

In a second step, the contribution of one or several spherical particles in interaction with the slab is included. This is done numerically using the coupled dipole method.[42] In this approach, each particle is properly discretized, each cell of the discretization mesh being equivalent to an electric point dipole with a given polarizability $\alpha(\omega)$. Note that we have used a polarizability including radiation reaction so that energy conservation (or the optical theorem) is exactly satisfied.[29,42] The electromagnetic response of the spheres is described by the collective response of the set of N induced dipoles. The electric field polarizing dipole number j (such that $\mathbf{p}_j = \alpha(\omega)\epsilon_0\mathbf{E}_{\mathrm{exc},j}$) can be written in a self-consistent way:

$$\mathbf{E}_{\mathrm{exc},j} = [\mathbf{G}_0(\mathbf{r}',\mathbf{r}) + \mathbf{S}_{\mathrm{slab}}(\mathbf{r}',\mathbf{r})]\cdot\mathbf{p} + \alpha(\omega)\epsilon_0\sum_{j\neq k}[\mathbf{G}_0(\mathbf{r}_j,\mathbf{r}_k) + \mathbf{S}_{\mathrm{slab}}(\mathbf{r}_j,\mathbf{r}_k)]\cdot\mathbf{E}_{\mathrm{exc},k} + \alpha(\omega)\epsilon_0\mathbf{S}_{\mathrm{slab}}(\mathbf{r}_j,\mathbf{r}_j)\mathbf{E}_{\mathrm{exc},j}. \tag{A2}$$

In this equation, $\mathbf{p}$ is a classical dipole placed at the position of the quantum emitter, acting as an external source producing the incident field. Equation (A2) is valid for each of the N dipoles comprising the system, defining hence a set of self-consistent linear equations. Once the system is solved for all polarizing fields, the total fields at any position can be obtained as a linear superposition of the fields radiated by each induced dipole. This allows to calculate the full decay rate Γ by computing the scattered field at the source position. One can also evaluate the total power emitted into the far field and obtained the radiative decay rate Γ^R. By subtraction, the nonradiative decay rate Γ^{NR} can be deduced, as well as the apparent quantum yield.

Finally, let us note that for exciting fields that do not vary appreciably on the scale of a spherical particle, the latter can be described by a single dipole, hence simplifying the calculations. In the present work we have worked under this approximation. Moreover, it is worth pointing out that the present method can be used with multilayered substrates and with systems involving only scatterers of finite size. Hence it is well suited to the study of complex three-dimensional geometries, including disordered systems.[43,44]

[1] R. Alléaume, F. Treussart, J.-M. Courty, and J.-F. Roch, New J. Phys. **6**, 85 (2004).
[2] X. S. Xie and R. C. Dunn, Science **265**, 361 (1994).
[3] P. Anger, P. Bharadwaj, and L. Novotny, Phys. Rev. Lett. **96**, 113002 (2006).
[4] T. Pons, I. L. Medintz, K. E. Sapsford, S. Higashiya, A. F. Grimes, D. S. English, and H. Mattoussi, Nano Lett. **7**, 3157 (2007).
[5] J. Seelig, K. Leslie, A. Renn, S. Kühn, V. Jacobsen, M. van de Corput, C. Wyman, and V. Sandoghdar, Nano Lett. **7**, 685 (2007).
[6] S. Lee, J. H. Ryu, K. Park, A. Lee, S.-Y. Lee, I.-C. Youn, C.-H. Ahn, S. M. Yoon, S.-J. Myung, D. H. Moon, X. Chen, K. Choi, I. C. Kwon, and K. Kim, Nano Lett. **9**, 4412 (2009).
[7] S. Kühn, U. Håkanson, L. Rogobete, and V. Sandoghdar, Phys. Rev. Lett. **97**, 017402 (2006).
[8] F. D. Stefani, K. Vasilev, N. Bocchio, N. Stoyanova, and M. Kreiter, Phys. Rev. Lett. **94**, 023005 (2005).
[9] P. Andrew and W. L. Barnes, Science **306**, 1002 (2004).
[10] K. Kneipp, Y. Wang, H. Kneipp, L. T. Perelman, I. Itzkan, R. R. Dasari, and M. S. Feld, Phys. Rev. Lett. **78**, 1667 (1997).
[11] E. Hao and G. C. Schatz, J. Chem. Phys. **120**, 357 (2004).
[12] J. Aizpurua, G. W. Bryant, L. J. Richter, F. J. García de Abajo, B. K. Kelley, and T. Mallouk, Phys. Rev. B **71**, 235420 (2005).
[13] S. Foteinopoulou, J. P. Vigneron, and C. Vandenbem, Opt. Express **15**, 4253 (2007).
[14] A. M. Funston, C. Novo, T. J. Davis, and P. Mulvaney, Nano Lett. **9**, 1651 (2009).
[15] P. Johansson, H. Xu, and M. Käll, Phys. Rev. B **72**, 035427 (2005).
[16] A. L. Demming, F. Festy, and D. Richards, J. Chem. Phys. **122**, 184716 (2005).
[17] S. Gerber, F. Reil, U. Hohenester, T. Schlagenhaufen, J. R. Krenn, and A. Leitner, Phys. Rev. B **75**, 073404 (2007).
[18] G. Baffou, C. Girard, E. Dujardin, G. Colas des Francs, and O. J. F. Martin, Phys. Rev. B **77**, 121101(R) (2008).
[19] J. P. Kottmann and O. J. F. Martin, Opt. Lett. **26**, 1096 (2001).
[20] P. Nordlander, C. Oubre, E. Prodan, K. Li, and M. I. Stockman, Nano Lett. **4**, 899 (2004).
[21] T. Atay, J.-H. Song, and A. V. Nurmikko, Nano Lett. **4**, 1627 (2004).
[22] V. V. Klimov and D. V. Guzatov, Phys. Rev. B **75**, 024303 (2007).
[23] W. Rechberger, A. Hohenau, A. Leitner, J. R. Krenn, B. Lamprecht, and F. R. Aussenegg, Opt. Commun. **220**, 137 (2003).
[24] F. Le, N. Z. Lwin, J. M. Steele, M. Käll, N. J. Halas, and P. Nordlander, Nano Lett. **5**, 2009 (2005).
[25] D. V. Guzatov and V. V. Klimov, Chem. Phys. Lett. **412**, 341 (2005).
[26] L. Rogobete, F. Kaminski, M. Agio, and V. Sandoghdar, Opt. Lett. **32**, 1623 (2007).
[27] V. Yannopapas and N. V. Vitanov, J. Phys.: Condens. Matter **19**, 096210 (2007).
[28] J. M. Wylie and J. E. Sipe, Phys. Rev. A **30**, 1185 (1984).
[29] R. Carminati, J. J. Greffet, C. Henkel, and J. M. Vigoureux, Opt. Commun. **261**, 368 (2006).
[30] G. W. Ford and W. H. Weber, Phys. Rep. **113**, 195 (1984).
[31] I. A. Larkin, M. I. Stockman, M. Achermann, and V. I. Klimov, Phys. Rev. B **69**, 121403(R) (2004).
[32] R. Castanié, M. Boffety, and R. Carminati, Opt. Lett. **35**, 291 (2010).
[33] S. Bidault, F. J. García de Abajo, and A. Polman, J. Am. Chem. Soc. **130**, 2750 (2008).
[34] J. Azoulay, A. Débarre, A. Richard, and P. Tchénio, Europhys. Lett. **51**, 374 (2000).
[35] M. Thomas, J.-J. Greffet, R. Carminati, and J. R. Arias-Gonzales, Appl. Phys. Lett. **85**, 3863 (2004).
[36] H. Mertens, A. F. Koenderink, and A. Polman, Phys. Rev. B **76**, 115123 (2007).
[37] D. Sarid, Phys. Rev. Lett. **47**, 1927 (1981).
[38] H. Raether, *Surface Plasmons on Smooth and Rough Surfaces and on Gratings* (Springer-Verlag, Berlin, 1988).
[39] L. S. Froufe-Pérez and R. Carminati, Phys. Rev. B **78**, 125403 (2008).
[40] J. E. Sipe, J. Opt. Soc. Am. B **4**, 481 (1987).
[41] J. J. Greffet and R. Carminati, Prog. Surf. Sci. **56**, 133 (1997).
[42] B. T. Draine, Astrophys. J. **333**, 848 (1988).
[43] A. Rahmani, P. C. Chaumet, F. de Fornel, and C. Girard, Phys. Rev. A **56**, 3245 (1997).
[44] L. S. Froufe-Pérez, R. Carminati, and J. J. Sáenz, Phys. Rev. A **76**, 013835 (2007).